

A NOMPC-Dependent Membrane-Microtubule Connector Is a Candidate for the Gating Spring in Fly Mechanoreceptors

Xin Liang,¹ Johnson Madrid,¹ Roland Gärtner,²
Jean-Marc Verbavatz,¹ Christoph Schiklenk,¹
Michaela Wilsch-Bräuninger,¹ Aliona Bogdanova,¹
Florian Stenger,² Axel Voigt,² and Jonathon Howard^{1,*}

¹Max-Planck Institute of Molecular Cell Biology and Genetics,
01307 Dresden, Germany

²Institut für Wissenschaftliches Rechnen, TU-Dresden,
01069 Dresden, Germany

Summary

Background: Mechanoreceptors contain compliant elements, termed “gating springs,” that transfer macroscopic stimuli impinging on the cells into microscopic stimuli that open the mechanosensitive channels. Evidence for gating springs comes from mechanical experiments; they have not been identified molecularly or ultrastructurally.

Results: We show that the filamentous structures that connect the plasma membrane to the microtubules are compliant structural elements in the mechanoreceptive organelle of fly campaniform receptors. These filaments colocalize with the ankyrin-repeat domain of the transient receptor potential (TRP) channel NOMPC. In addition, they resemble the purified ankyrin-repeat domain in size and shape. Most importantly, these filaments are nearly absent in *nompC* mutants and can be rescued by the *nompC* gene. Finally, mechanical modeling suggests that the filaments provide most of the compliance in the distal tip of the cell, thought to be the site of mechanotransduction.

Conclusions: Our results provide strong evidence that the ankyrin-repeat domains of NOMPC structurally contribute to the membrane-microtubule connecting filaments. These filaments, as the most compliant element in the distal tip, are therefore good candidates for the gating springs.

Introduction

The sensing of sound, touch, and acceleration in cells requires the conversion of mechanical stimuli into electrical signals [1, 2]. This process, known as mechanotransduction, occurs much more rapidly than other sensory processes, such as phototransduction or chemotransduction [2, 3]. The short delay suggests that the ion channels that mediate mechanotransduction are directly gated by force [2, 4].

To directly couple mechanical stimuli to ion channels, Corey and Hudspeth hypothesized that the transduction apparatus contains a set of linked mechanical components that convert the deformation of a cell into a force that acts on the mechanotransduction channels [5]. The opening of the channel’s gate partially relieves this force, thereby biasing the channel’s probability of being open. This mechanical system needs to be compliant for two reasons. First, compliance is required to match the mechanical impedance of the cytoskeleton and extracellular matrix, which give rigidity to the cell, to that of

the transduction channels, which are likely to be much softer. Second, compliance allows a single channel to open and close even when the deformation is fixed, thereby transducing cell deformation into a graded signal, namely the channel’s opening probability. If the compliance of the mechanical system is primarily determined by one of the components, then we refer to this component as a “gating spring.” Evidence for gating springs comes from mechanical and electrophysiological studies [6–8]. However, no gating spring has been identified at the molecular or ultrastructural level.

Efforts have been made to identify gating springs in various model systems. In vertebrate hair cells, the tip link, the initial candidate for the gating spring [7, 9], was found to be composed of cadherin 23 and protocadherin 15, suggesting that it would be too rigid to function as a gating spring [3, 10–12]. The plasma membrane and a postulated intracellular tether are proposed as alternative candidates [3, 13–15], but direct evidence is still lacking. In another model of mechanotransduction, the posterior lateral microtubule cells of *C. elegans*, there is an intracellular filament between the membrane and the microtubules at the site of mechanotransduction [16]. Because this filament has no direct connection with the transduction channel, it was suggested that the filament activates mechanosensitive channels by deforming the plasma membrane [16]. As in the case of hair cells, however, it is not clear which structural element is the source of the compliance in the transduction apparatus.

In the case of fly bristle and campaniform mechanoreceptors, ultrastructural analysis has shown that the distal tip of the cilium, thought to be the site of mechanotransduction, contains a filamentous structure, termed the “membrane-integrated cone” [17, 18]. The filaments link the plasma membrane to the microtubules. The filaments are oriented parallel to the excitatory-inhibitory axis of the cell and change their length dramatically in response to cuticle deformations [19]. These observations suggested that the filaments might be compliant structures that convey mechanical forces to membrane channels. However, the molecular identity of these filaments is unclear, preventing further investigation of their potential role as gating springs.

NOMPC, a candidate mechanotransduction channel [20, 21] (but see [22]), has an ankyrin-repeat domain that has been hypothesized to be a gating spring in fly bristle and campaniform receptors [23], based on its predicted helical structure and its presumed compliance [11, 24]. Although NOMPC was found to be essential for mechanical processes associated with transduction [25–27] in fly auditory mechanoreceptors, there is no direct evidence for the hypothesis that the ankyrin-repeat domain is the gating spring. On the other hand, the ankyrin-repeat domain functions as a localization domain for the NOMPC channel [28], consistent with ankyrin-repeats being protein-protein interaction domains [29]. Thus, whether the ankyrin-repeat domain of NOMPC functions as a gating spring, in addition to its role in localization, remains to be demonstrated.

To elucidate the function of the ankyrin-repeat domain of NOMPC in mechanotransduction, we investigated the ultrastructure of campaniform mechanoreceptors in *nompC* mutants. We found that the membrane-microtubule connecting

*Correspondence: howard@mpi-cbg.de



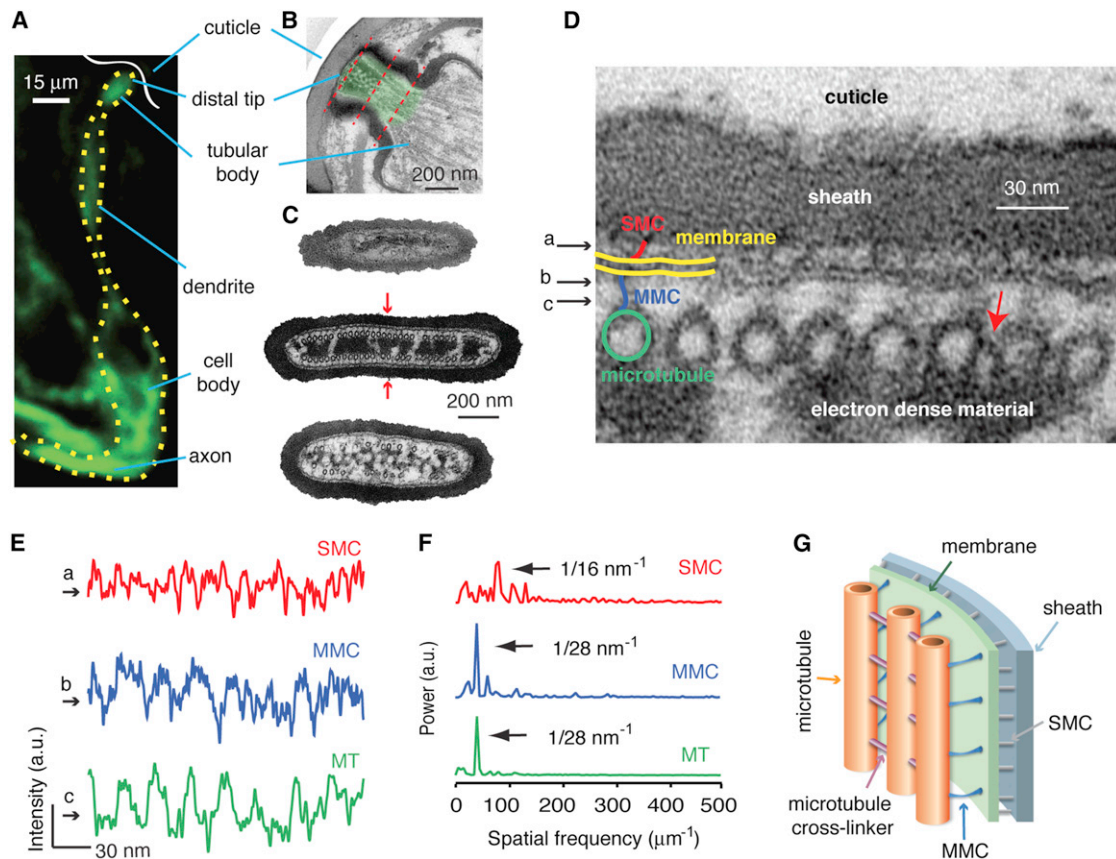


Figure 1. The Distal Tip of Campaniform Mechanoreceptors Has an Ordered Ultrastructure

(A) A campaniform mechanoreceptor was labeled by neuronal expression of GFP-tubulin (*uas-gfp-tubulin; elav-gal4*). The yellow dotted line outlines the receptor cell. The white line indicates the position of the cuticle.
 (B) A transmission electron micrograph of a longitudinal section of the distal tip region (green). The three red dashed lines indicate the planes of the sections shown in (C).
 (C) Cross-sections of the distal tip region in different positions (upper, most distal; lower, most basal) have different shapes. The two red arrows in the middle panel indicate the directions of the force that activates the campaniform mechanoreceptor (i.e., the excitatory-inhibitory axis) [17, 31].
 (D) A transmission electron micrograph showing the ultrastructure in the distal tip: microtubules (green), membrane-microtubule connectors (MMC, blue), membrane (yellow), sheath-membrane connectors (SMC, red), sheath and the cuticle. The red arrow indicates a cross-linker between adjacent microtubules. The arrows on the left (a, b and c) indicated the regions corresponding to the line-profiles shown in (E).
 (E) The line profiles of the microtubules, MMCs and SMCs in the regions indicated in (D).
 (F) The power spectra of the line-profiles in (E) have peaks. The numbers indicate the average spatial frequencies of SMCs, MMCs and microtubules from ten cells.
 (G) A schematic of the ultrastructure in the distal tip.

filaments were nearly absent in *nompC* null mutants, that the ankyrin-repeat domain colocalizes with the filaments by immunoelectron microscopy (immuno-EM), and that the size and shape of the filament match those of purified ankyrin-repeat domains. These experiments therefore suggest that the ankyrin-repeat domains contribute structurally to the filaments. Additional genetic and ultrastructural experiments, as well as mechanical modeling, suggest that the filaments are the most compliant structure in the distal tip, providing evidence that they might serve as gating springs.

Results

The Distal Tip of the Campaniform Receptor Has a Highly Ordered Ultrastructure

Campaniform mechanoreceptors (Figure 1A) are enriched in fly halteres (see Figure S1 available online) [30]. They respond to mechanical stimuli impinging on the cuticle that overlays the

distal tip of the neuron (green in Figures 1B and S1). Transmission electron microscopy (TEM) shows that the cross-section of the distal tip has an elliptical shape (Figure 1C). In the cross-section, there is a highly organized cytoplasmic structure containing two rows of microtubules with electron-dense material (EDM) in between (middle panel in Figure 1C). The distal tip contains four major structural elements: the extracellular sheath, the plasma membrane, two rows of microtubules, and the EDM (Figure 1D). In addition, we observed three types of cross-linkers. The first type connects the microtubules to the plasma membrane (blue in Figure 1D). We term this filament the “membrane-microtubule connector” (MMC). It corresponds to the membrane-integrated cone mentioned in the Introduction [17, 18], but because it is neither integral to the membrane nor conical, we have renamed it to reflect its localization (see Supplemental Results, Note S1). The second type of cross-linker, which we term the “sheath-membrane connector” (SMC) (Supplemental Results, Note S1), is located between

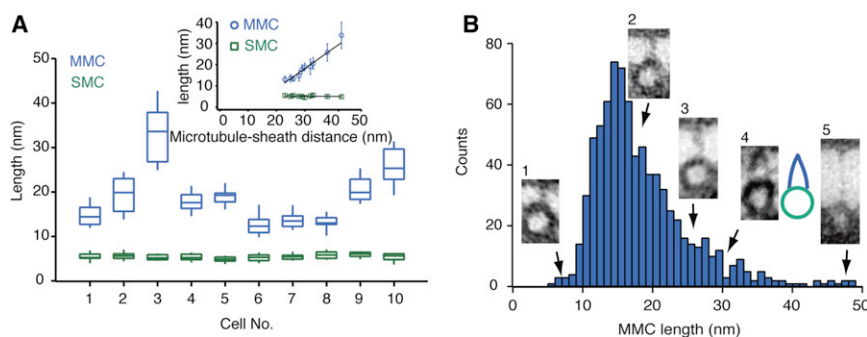


Figure 2. The Length Distributions of the Membrane-Microtubule Connectors and the Sheath-Membrane Connectors

(A) The lengths of the MMCs (blue) and the SMCs (green) measured in ten cells. Inset: the lengths of MMCs and SMCs are plotted against the microtubule-sheath distance measured in the same cell. (B) The end-to-end lengths of MMCs showed a broad range. Representative images of MMCs in different lengths are shown in the insets (1: ~10 nm; 2: ~20 nm; 3: ~25 nm; 4: ~35 nm; 5: ~50 nm). An example of a helical MMC is shown in inset 3. An example of two MMCs associated with a single microtubule in one section and a schematic are shown in inset 4.

the membrane and the extracellular sheath (red line in Figure 1D) [17]. The third type (red arrow in Figure 1D), which we term the “microtubule crosslinker,” has not been described before and connects the microtubules within each row into small arrays. These three crosslinkers link the plasma membrane, the sheath, and the microtubules, thereby providing a structural basis for the transfer of mechanical force inside the distal tip, thought to be the mechanotransduction organelle of the receptor.

Because the MMCs and SMCs were difficult to resolve in our TEM micrographs, we used image analysis to obtain objective evidence to confirm their existence and to measure their periodicity. Intensity profiles (Figure 1E) along lines in the regions of interest (black arrows in Figure 1D) were Fourier transformed. The resulting power spectra showed peaks (Figure 1F) that were significantly higher than the background (see Experimental Procedures), confirming that the MMCs and SMCs formed periodic structures. The line profiles of the MMCs correlated with those of the microtubules and had a similar spatial period (MMC: 27.9 ± 2.9 nm; microtubule: 28.0 ± 3.3 nm; mean \pm SD, $n = 10$ cells) (Figure 1F). In contrast, the SMCs had a smaller spatial period (15.9 ± 3.9 nm; mean \pm SD, $n = 10$ cells). Though the ratio of the SMC and MMC periods was not significantly different from 2, two lines of evidence suggest that the SMCs and the MMCs do not share a common lattice. First, many MMCs were not aligned with SMCs (and vice versa). Note that the SMCs in alignment with the MMCs may not be in the same z plane (the TEM micrographs are 2D projections of the 50 nm thick sections). Second, SMCs were present in the spaces corresponding to the gaps between microtubule arrays; because there are no MMCs in these gaps, it is unlikely that the SMCs make direct structural connections with the MMCs. Based on our observations and analysis, as well as those described in the literature [17–19], we propose a structural model for the distal tip of the campaniform mechanoreceptor (Figure 1G).

Membrane-Microtubule Connectors Appear to Be Relatively Compliant Structures

Given that the MMCs and SMCs make a direct contact to the plasma membrane and are suitably positioned to be candidates for the gating springs (they are oriented perpendicular to the membrane and therefore parallel to the excitatory-inhibitory axis of the cell, indicated by the red arrows in the middle panel in Figure 1C [31]), we asked whether they are compliant structures. The end-to-end lengths of MMCs and SMCs were measured in ten cells where the SMCs and MMCs were both clearly visible. The lengths of MMCs in these ten cells showed a large variation (18.9 ± 6.5 nm, $n = 10$ cells, mean \pm SD, SD/mean = 0.32) (Figure 2A), which we further

confirmed by measuring more MMCs in 23 cells (18.7 ± 8.3 nm, mean \pm SD, $n = 794$ MMCs) (Figure 2B). In the same ten cells, the lengths of SMCs were more consistent (5.1 ± 0.3 nm, $n = 10$ cells, mean \pm SD, SD/mean = 0.06) (Figure 2A). One-way ANOVA analysis showed that the mean lengths of the MMCs in these ten cells were significantly different ($p < 0.001$), whereas those of the SMCs were not ($p > 0.05$). In addition, we found that the lengths of MMCs showed a linear correlation with the microtubule-sheath distance (inset in Figure 2A), which varied considerably, perhaps due to different strains in different receptors during tissue preparation. The slope of this linear correlation (0.96), being close to unity, suggests that most of the changes in microtubule-sheath distances were taken up by the length changes of the MMCs. In contrast, the lengths of SMCs did not vary with the microtubule-sheath distance (inset in Figure 2A). These observations suggest that the MMCs are more compliant, whereas SMCs are stiffer.

MMCs Colocalize with the Ankyrin-Repeat Domain of NOMPC

Because the ankyrin-repeat domain of NOMPC was proposed to form the MMC [23], we asked whether they colocalize. We used an *elav-gal4* line to drive neuronal expression of GFP-tubulin to mark the microtubules in the distal tip (Figure 3A, upper panel). Using a monoclonal antibody against the first nine ankyrin repeats at the N terminus of NOMPC [30], we found that the immunofluorescence signal of NOMPC (Figure 3A, middle panel) superimposed with that of the microtubules in the distal tip of the campaniform receptor (Figure 3A, lower panel). This overlap shows that the ankyrin-repeat domains of NOMPC (the antigenic site) and the MMCs colocalize within the spatial resolution of the light microscope. Furthermore, immuno-EM using the same antibody confirmed the close proximity of the ankyrin-repeat domain to the microtubules. MMCs were not as clearly visible and regular in immuno-EM micrographs as in conventional TEM micrographs (Figure 3B, upper panel), due to the omission of the OsO_4 contrasting step and the weaker fixation for preservation of antigenicity. The NOMPC-antibody-labeled gold particles preferentially localized to the distal tip regions: intracellular and sheath had a density of 38.5 ± 14.5 particles/ μm^2 , whereas outside the sheath the density was 8.6 ± 4.6 particles/ μm^2 ($p < 0.001$, Welch’s t test; $n = 16$ sections). To compare the localization of gold particles within the cells, we linearly transformed TEM images of distal tips to fit a 50×10 grid (Figure 3B, middle panel). Then, the gold particles from all images were mapped to a schematic (Figure 3B, lower panel). More than 75% of the gold particles were located within the MMC region between the membrane and the microtubules (Figure 3B).

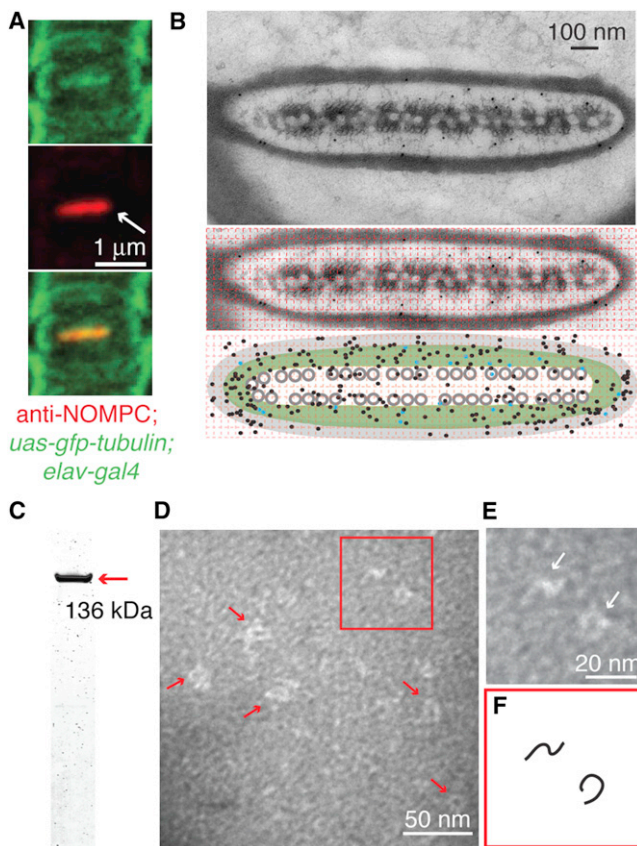


Figure 3. Membrane-Microtubule Connectors Colocalize with the NOMPC Ankyrin-Repeat Domain and Resemble Its Shape

(A) The microtubule fluorescence in the upper panel (green, *uas-gfp-tubulin*; *elav-gal4*) overlapped with NOMPC fluorescence in the middle panel (white arrow; red, anti-NOMPC antibody [30]) as shown in the superposition (lower panel). This is the top view of the distal tip region of the campaniform receptor (as in Figure 1C). The green color outside the distal tip region in the upper panel is the autofluorescence from the cuticle.
 (B) Immuno-EM using an anti-NOMPC antibody in cross-sections of a distal tip. Upper panel: a representative immuno-EM image showing that the gold particles are mainly found within the cell. Middle panel: a 50×10 grid was superimposed on the micrograph of distal tip. Lower panel: the positions of all gold particles observed in 16 images (four cells and four sections per cell) were mapped onto the grid and shown in a schematic of the distal tip region. The blue particles in the lower panel are those shown in the upper panel.
 (C) SDS-PAGE of the purified N-terminal fragment of NOMPC (red arrow).
 (D) An EM micrograph of purified N-terminal fragment of NOMPC using negative staining. The red box indicates the enlarged region shown in (E).
 (E) Examples of helical and circular molecules (white arrows).
 (F) Schematics of the molecules in (E).

After taking into account the nonspecific binding of the gold particles to the sheath (see Supplemental Results, Note S2) and the sizes of the primary and secondary antibodies (10 nm for each antibody), we estimated that the chance that the epitope localized in the MMCs region is above 80% (Supplemental Experimental Procedures). Therefore, we conclude that the immune signal corresponds to the location of the MMCs. This is consistent with the predicted juxtamembrane, cytoplasmic location of the ankyrin-repeat domain [23].

MMCs Resemble the Ankyrin-Repeat Domain in Shape and Size

The ankyrin-repeat domain was predicted to form a helical structure [23] based on the crystal structure of 12 ankyrin-R

repeats [32]. In our micrographs, MMCs appeared to be filament-like structures, and some of them showed a helix-like structure (e.g. inset 3 in Figure 2B). Therefore, the shape of MMCs might resemble that of the ankyrin-repeat domain. To further test this possibility, we purified an N-terminal fragment of NOMPC (amino acids 1–1268, which includes the ankyrin-repeat domain 126–1143) (Figure 3C) and observed its shape using negative-staining electron microscopy. The particles on the EM grids were generally elongated and adopted curved shapes (arrows in Figure 3D). Helix-like structures (Figures 3E and 3F), resembling the side view of the ankyrin-repeat domain [23], and circle-like ones, resembling the top view [23] (Figures 3E and 3F), were observed. The variation in shape may be due to (1) different orientations of the ankyrin-repeat domains on the grid and (2) deformations during sample preparation. The contour length of the filaments was 20.5 ± 3.8 nm ($n = 32$, mean \pm SD). Given the likely deformation of the protein and the fact that the TEM micrographs are 2D projections, the length of the purified ankyrin-repeat domain we measured is consistent with the estimated contour length of 29 ankyrin repeats (~ 26 nm) [11]. Though the detailed 3D structure of NOMPC ankyrin-repeat domain needs to be further investigated, our micrographs suggest that it is filamentous and curved, consistent with the shape and length of the MMCs.

MMCs Are Dependent on the Presence of NOMPC

The colocalization of MMCs and the NOMPC ankyrin-repeat domain and their similarity in size and shape suggest that the ankyrin-repeat domain might structurally contribute to the MMCs. To test this hypothesis, we analyzed the ultrastructure of *nompC* mutants (Figure 4A). We first studied *nompC³*, a null mutant of *nompC*. The control strain (*cn,bw*) (Figure 4B, upper left panel) showed a normal response to mechanical stimuli and was ultrastructurally identical to wild-type. In contrast, *nompC³* flies showed no response to mechanical stimulation (Figure 4B, upper right panel). MMCs were greatly reduced in number in *nompC³* mutants, whereas the microtubules appeared normal and SMCs were present (Figure 4B, upper right panel). The functional and ultrastructural defects were rescued by crossing the *nompC³* mutant to a transgenic fly carrying a *p[acman]* construct containing the *nompC* gene (Figure 4B, lower left panel; Figure S2).

We also studied the *nompC⁴* (C1400Y) mutant. Interestingly, we found that the immunolocalization patterns of NOMPC in campaniform receptors, bristle receptors, and scolopidial cells were all differently affected by the C1400Y mutation (Figure S3), consistent with an earlier report [33]. In campaniform mechanoreceptors of *nompC⁴* flies, NOMPC immunolabeling was present but weaker (compared to wild-type) in the distal tip, suggesting there were fewer NOMPC molecules there. MMCs were still present in the distal tip of the *nompC⁴* mutant, but the number was significantly reduced (lower right panel in Figure 4B). The intermediate phenotypes observed by immunofluorescence microscopy and TEM were paralleled by an electrophysiological phenotype that was intermediate between wild-type and *nompC³* (Figure 4B, lower right panel). Therefore, the more NOMPC molecules in the distal tip, the more MMCs were observed and the stronger the electrophysiological responses were.

Power spectral analysis of *nompC³* and *nompC⁴* mutants showed no periodic signals in the MMC region, whereas control flies (*cn,bw*) and rescued flies showed similar periodic signals to wild-type (Figure S4). Unbiased evaluation of the phenotypes was undertaken by five investigators who counted

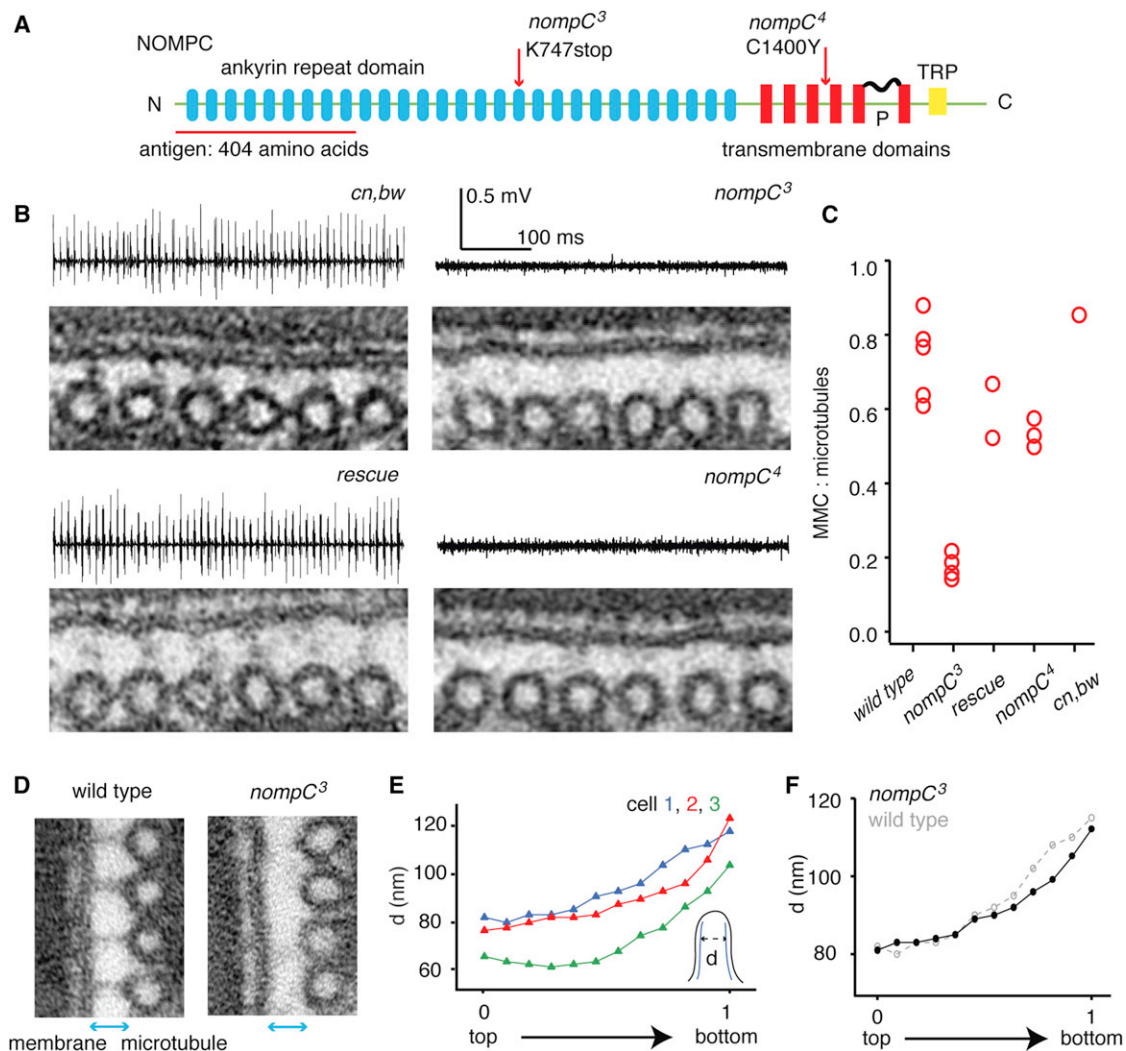


Figure 4. Membrane-Microtubule Connectors Depend on NOMPC

(A) A schematic of the NOMPC protein structure. The arrows mark the positions and amino acid changes in *nompC³* and *nompC⁴*. The red line indicates the position of the peptide antigen.

(B) Representative TEMs of the distal tips from the indicated fly strains. The corresponding electrophysiological data from the flies with the same genotype are shown above the corresponding micrographs. *rescue*, *nompC³*; *p[acman]*, *CH321-17B03*.

(C) The number of MMCs and microtubules in different flies were counted, and the ratio between the MMCs and the microtubules (MMC, microtubule) was calculated. Each data point in the figure is the average value of many sections from one fixation (wild-type: 5 fixations, 14 cells, 25 sections; *nompC³*: 4 fixations, 18 cells, 28 sections; *rescue*: 2 fixations, 6 cells, 10 sections; *nompC⁴*: 3 fixations, 10 cells, 20 sections; *cn,bw*: 1 fixation, 2 cells, 5 sections).

(D) The membrane-microtubule distance in wild-type and *nompC³* mutant flies is similar.

(E) The distances (*d*) between the two rows of microtubules were measured in three series of cross sections of the distal tips. The values of *d* (solid triangle) are plotted against the *z* positions of the sections in the series. Different colors correspond to measurements from different cells. The inset is a schematic based on cell 1.

(F) The same plot of *d* values as (E) measured in a *nompC³* mutant. Cell 1 in (E) is shown in gray with dashed line as a control.

the number of MMCs and microtubules in a mixed sample of TEM images from different mutants (without knowing which strains the images came from). Based on these “blind” experiments, the MMC: microtubule ratio was calculated and used for statistical analysis (Figure 4C). In wild-type and control flies (*cn,bw*), the MMC: microtubule ratio was in the range of 0.60–0.90. *nompC³* had a MMC: microtubule ratio of 0.10–0.20 ($p < 0.001$, Welch’s *t* test), whereas *nompC⁴* had a ratio of 0.45–0.60 ($p < 0.05$ compared to wild-type, Welch’s *t* test). In rescued *nompC³* flies, the MMC: microtubule ratio increased to 0.50–0.70. Taken together, these results indicated that NOMPC is required for the localization or integrity of the MMCs.

The finding that almost all MMCs were missing in the *nompC³* mutant allowed us to further evaluate the roles of the MMCs in forming or maintaining the structural integrity of the distal tip. If the MMCs act as rigid spacers, then removing them should lead to a change in the membrane-microtubule distance. However, this distance did not change in the *nompC³* mutant (wild-type: 16.1 ± 5.3 nm, $n = 23$ cells; *nompC³*: 16.6 ± 4.2 nm, $n = 19$ cells; $p = 0.75$, Welch’s *t* test) (Figure 4D). Although the mechanism that sets the membrane-microtubule distance is not clear, it seems that it is not the MMCs that hold the membrane and the microtubules together or keep them apart. Another structural feature of the distal tip is that microtubules in wild-type flies bend

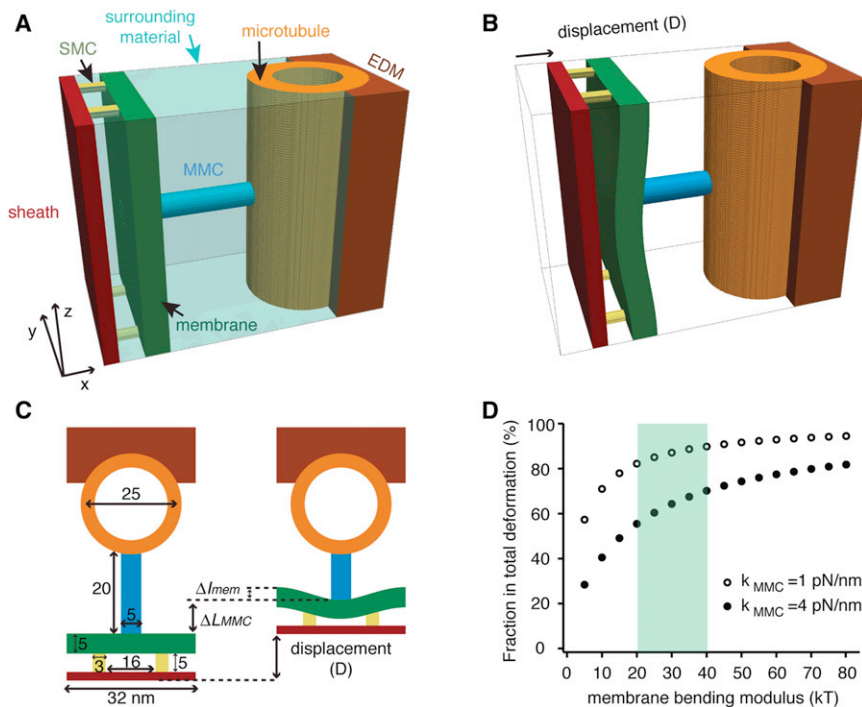


Figure 5. Finite-Element Model of the Distal Tip Suggests that the MMCs Are the Most Compliant Elements

(A) The geometrical organization of the structural elements of the model.

(B) 3D schematic showing the deformation of the transduction apparatus under a stimulus (the displacement of the sheath). Note that the surrounding material is omitted in this panel.

(C) 2D schematic of the transduction apparatus (unit: nm). The parameters (D , Δl_{mem} , and ΔL_{MMC}) are labeled.

(D) The fractional contributions of the MMC ($\Delta L_{MMC}/D$, circle plots) in response to stimulation. The region highlighted in green shows the best-estimate range of membrane stiffnesses based on the literature ($\kappa = 20\text{--}40\text{ kT}$ where k is the Boltzmann constant and T is the absolute temperature). In these simulations, the spring constant of the MMC was 1.0 pN/nm (open) or 4.0 pN/nm (closed).

outward at the proximal end (Figure 4E; also see Figure 1C for an example). If MMCs exert forces to bend the microtubules, there should be no microtubule bending when MMCs are absent. However, the bending of the microtubules was not affected in *nompC*³ mutants (Figure 4F), suggesting the MMCs do not pull the microtubules and the membrane together. In summary, the removal of MMCs had no major effects on the overall shape of the distal tip, consistent with their being relatively compliant elements in the system.

MMCs Are the Most Compliant Element in the Transduction Apparatus

To determine whether MMCs are the major source of the compliance in the transduction apparatus, as expected if they are the gating springs, we took a modeling approach. A mechanical model of the mechanotransduction apparatus was built based on our ultrastructural studies (Figure 5A). We assigned a mechanical stiffness to each element based primarily on values from the literature. Then, we used a finite-element method to determine the strain in each element under an imposed displacement of the sheath (Figure 5B). Based on the predicted stiffness of the ankyrin-repeat domain, the stiffness of the MMCs was set to 1.0 pN/nm (monomeric form) and 4.0 pN/nm (tetrameric form) [11, 23, 24]. Due to the uncertainty about the mechanical properties of the plasma membrane, we investigated a range of bending stiffnesses of the bilayer from 10 kT to 80 kT (k is the Boltzmann constant; T is the absolute temperature) [13, 34, 35]. A range of Young's modulus of SMCs (from 0.005 GPa to 2 GPa) was also investigated. The Young's modulus of the microtubules was set to 2 GPa [36]. Because the EDM and the sheath are likely to be stiff structures, we assigned them the same Young's modulus as the microtubule.

We found that when the whole structure was compressed, most of the deformation occurred as a length reduction of the MMC (ΔL_{MMC}) and an indentation of the membrane (Δl_{mem}) (Figure 5C). To quantify their contributions to the total

deformation, we calculated the fractional deformation of each component (Figure 5C). If the stiffness of MMCs is 1 pN/nm, the simulations showed that the length changes of MMCs are a major source of the deformation in the system over the range of membrane-bending stiffnesses considered (Figure 5D, open circles). In the highlighted region (green) of our best estimate of the membrane-bending stiffness (20 kT to 40 kT), the MMCs contributed 80%–90% of the total deformation. When we increased the stiffness of the MMCs to 4 pN/nm, the MMCs still contributed more than 50% of the total deformation when the membrane stiffness is in our best-estimate range (Figure 5D, closed circles). Most of the remaining deformation was in the membrane. Note that any resting tension in the membrane, which was not incorporated into the current model, is expected to stiffen the membrane and further increase the contribution of MMCs to the total compliance. The SMCs themselves made only a small contribution to the total deformation even when their Young's modulus was reduced to 0.005 GPa, indicating that they are not a major source of compliance in the system. However, in some cases where the SMCs are in alignment with the MMCs (Figure 1D), the plasma membrane is expected to have a smaller deformation. In this scenario, the MMCs contribute even more to the total compliance. The other structures contribute negligibly to the overall compliance. Therefore, our simulations show that the MMCs are expected to provide most of the compliance in the transduction apparatus, further supporting our hypothesis that MMCs serve as the gating springs.

Discussion

The Ankyrin-Repeat Domain Structurally Contributes to MMCs

Based on our experiments, we propose that the ankyrin-repeat domain of NOMPC structurally contributes to the filamentous MMCs. This proposal is based on the following observations and arguments. The crucial observation is that the MMCs depend on the presence of NOMPC. Although it is formally possible that NOMPC is only required for the

assembly or maintenance of the MMCs, several observations suggest that the NOMPC protein contributes directly to the MMC. (1) Antibodies to the ankyrin-repeat domain of NOMPC colocalize with the MMCs by light microscopy and immunoelectron microscopy (Figure 3). (2) The length of the MMC is similar to the predicted length of the ankyrin-repeat domain [23, 24, 32]. Furthermore, the purified NOMPC ankyrin-repeat domain has a similar shape and length to the MMCs (Figure 3). (3) The more NOMPC molecules in the distal tip, the more MMCs (wild-type > *nompC⁴* > *nompC³*, Figure 4). (4) The ankyrin-repeat domain of NOMPC is a microtubule-association domain [28] and is therefore predicted to span from the membrane to the microtubule, as the MMC does. (5) The overall molecular mass of the ankyrin-repeat domain, up to 500 kDa if the NOMPC proteins form a tetramer, is large enough to be visualized by TEM; thus, we expect to see the ankyrin-repeat domain in the region where the MMC is observed by TEM. Therefore, genetic and microscopic evidence suggest that the ankyrin-repeat domain of NOMPC structurally contributes to the MMC.

A potential caveat to our conclusion that NOMPC is an essential component in the MMC complex is that in *nompC³* mutants about 10% of the filamentous connections remain (Figure 4C). We do not know what these structures are. The Fourier analysis shows no periodicity in the MMC region in *nompC* null mutants, suggesting the remaining connecting structures are not related to the NOMPC-dependent MMCs. The low abundance and irregularity of these NOMPC-independent connectors suggest that they might be the background “noise” formed by denatured proteins. A second possibility is that the MMCs are molecular complexes formed by the ankyrin-repeat domain of NOMPC and other molecules. When NOMPC is missing, the other components might form filament-like structures on their own, but only in rare cases. We think it is unlikely that a second transduction channel contributes the remaining filamentous structures in *nompC³* because mechanosensory responses were completely absent in the campaniform mechanoreceptors from *nompC³* mutants.

NOMPC-Dependent MMCs Might Serve as Gating Springs

Our results have shown that the MMCs appeared to be more compliant than the SMCs (Figure 2A). Having established that the ankyrin-repeat domains are likely to be a molecular component of the MMC complex, our work provides three new lines of evidence that the MMCs, being the most compliant structure in the system, might act as the gating springs. (1) *NompC* null mutants show that the NOMPC-dependent MMCs are not required for the overall shape of the distal tip of the campaniform receptor. The observation that the MMCs do not play a structural role is consistent with their being the most compliant structure in the distal tip. (2) Based on the predicted stiffness of the ankyrin-repeat domain, finite-element modeling indicates that the MMCs are the most compliant elements in the distal tip and are strained up to four times more than the membrane, the next most compliant element in the system. The modeling indicates that any conformational changes of the transduction channels (NOMPC or other channels) in response to transverse forces applied to the distal tip will be taken up primarily by the strain in the MMCs. This is precisely the definition of the gating spring. (3) NOMPC was recently found to form a subunit of a mechanotransduction channel in a heterologous system [20]. Our observations suggest that the MMCs might be mechanically

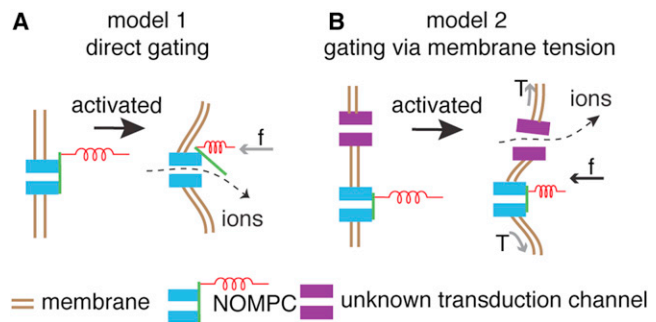


Figure 6. Two Models of Mechanotransduction

(A) Model 1: direct gating. NOMPC (blue) is the transduction channel and is activated by compressive force.

(B) Model 2: gating via membrane tension. A second, unknown, channel (purple) is the transduction channel and is activated by membrane tension. The gray arrows indicate the proximal forces acting on the transduction channels in (A) (compressive force, *f*) and (B) (membrane tension, *T*).

in series with the transduction channel, as expected if they are the gating spring.

Implications for the Identity of the Transduction Channel and Its Gating

Thus far, we have made no assertions about whether NOMPC is the transduction channel in campaniform receptors. If NOMPC is indeed the transduction channel, then it makes sense that the gating spring is a part of the channel protein, because the gating spring could convey force directly to the amino acids involved in channel gating (Figure 6A). Our observations and a recent report that NOMPC is a subunit of the mechanotransduction channel [20] directly support this simple and efficient model. However, our proposal that the MMC/ankyrin-repeat domain is the gating spring does not presuppose that NOMPC is the transduction channel. Note that Lehnert et al. argue that NOMPC is not the transduction channel in the case of the fly auditory cells [22]; however, our proposal implies that NOMPC is still essential for gating, which is the case for campaniform receptors, but not the case for auditory cells [22]. Though NOMPC is essential for transduction, it need not be the transduction channel, because our mechanical model shows that tension in the MMC leads to deformation and tension in the plasma membrane. A second channel located in the membrane, not necessarily even physically contacting NOMPC, could be opened by this increase in membrane tension (Figure 6B). The conformational change associated with the opening of this channel will reduce the tension in the membrane, which, in turn, will lessen the tension and strain in the MMC. In other words, the MMC can still be the most compliant element in the system and so act as the gating spring even if the proximal stimulus to the channel is membrane tension. Note that in this model, if there is no resting tension, then both positive and negative displacements of the sheath will lead to an increase in tension in the membrane; thus the channel response will be symmetric. In order to have a nonsymmetric response (i.e., inhibition in addition to excitation as observed), there has to be resting tension, which has not been included in our current finite-element model.

In conclusion, we argue that NOMPC, whether or not it is the transduction channel, is an essential component of the transduction apparatus through its contribution of the gating spring.

Experimental Procedures

Flies

All flies were maintained on standard medium at 23°C–25°C. *Oregon R* was used as the wild-type strain. *nompC*³ and *nompC*⁴ were provided by Martin Göpfert (University of Göttingen, Germany). All other fly stocks were from the Bloomington *Drosophila* Stock Center at Indiana University. The *P[acman]* clone, CH321-17B03, was from *Drosophila* Genetic Resource Center [37] and was injected into fly strain 9750 (PBac[yellow[+]-attP-3B]VK00033) (Bestgene). The recombination of *P[acman]* construct into the correct landing site was checked with PCR (Figure S2).

Conventional Transmission Electron Microscopy

Flies between 1 and 3 days posteclosion were used for imaging the ultrastructure of the campaniform receptors. The TEM protocol is based on the protocol described previously [30] and described in Supplemental Experimental Procedures.

For negative staining of purified protein, 3 μ l purified protein sample was applied to the carbon-coated EM copper grids and stained with 1% uranyl acetate. The negatively stained sample was imaged in a TECNAI 12 TEM operated at 100 kV, with a 2k TVIPS Camera (TVIPS).

Immunoelectron Microscopy

Flies between 1 and 3 days posteclosion were anesthetized with CO₂. The halteres were dissected and fixed in 4% paraformaldehyde in 0.1 M phosphate buffer at pH 7.4 for 1 hr at room temperature. The samples were sequentially dehydrated using a gradient series of 50, 70, 80, 90, 96, and 100% ethanol, 2 \times 20 min for each step. The final dehydration step in 100% ethanol was repeated three times. The samples were then infiltrated with LR white:ethanol mixtures of 1:2 and 2:1 for 1 hr each, followed by 100% LR white at room temperature for 20 min and 100% LR white overnight at 4°C. The next day, the samples were changed into 100% LR white at room temperature. The samples were flat embedded between two glass slides coated with Teflon, using appropriate spacers to avoid compression of the halteres. Then, the samples were incubated in an inert nitrogen chamber at 60°C for 36 hr. From these samples, ultrathin sections (thickness: 50 nm) were cut with a diamond knife on a Leica Ultracut S microtome and collected on Formvar-coated copper slot grids. The immunostaining of the sections followed the standard procedures (Supplemental Experimental Procedures). The sections were imaged in a TECNAI 12 transmission electron microscope (FEI, Netherlands) operated at 100 kV. The mapping and the density counting of the gold particles, as well as the measurements of the epitope region, were performed with Fiji (Supplemental Experimental Procedures).

Periodicity Measurements of the MMCs, the SMCs, and the Microtubules

The line profiles in the microtubule, the MMCs, and the SMCs regions were extracted from the TEM images with Fiji (<http://fiji.sc/wiki/index.php/Fiji>). The power spectra analysis of the line profiles was performed with MATLAB. Whether a particular peak in the power spectra is significant or not was examined at the significance level $\alpha = 0.05$ with Bonferroni correction [38]. When comparing the numbers of SMCs and MMCs in the distal tips, only the TEM micrographs in which the peaks of SMCs, MMCs, and microtubules were all considered to be significant were used to calculate the spatial frequency ($n = 10$ cells) shown in Figure 1F.

Blind Counting of the MMCs

To count the number of MMCs in an objective way, we mixed the TEM micrographs from different sample groups, and they were independently counted by five investigators. As a quality control, only spherical microtubules were taken into account (>80% of total microtubules). Furthermore, several mirrored images were included as internal controls to evaluate the consistency of each investigator. The ratios of MMCs to microtubules was calculated for each type of fly and used for statistical analysis.

Electrophysiology Recording

An extracellular recording setup was used to assay the function of campaniform mechanoreceptors of the haltere (Figure S1). The detailed methods of the signal recording and the data analysis were described in Supplemental Experimental Procedures.

Mechanical Analysis of the Membrane-Microtubule Connection

A finite-element method was used to model the mechanical behavior of the structural elements in the distal tip of the campaniform mechanoreceptor. The details of the finite-element model were described in the Supplemental Experimental Procedures.

Purification of N-Terminal Fragment of NOMPC

The coding region of the N-terminal fragment of NOMPC was modified by addition of an N-terminal maltose-binding protein tag (MBP-tag) and then expressed in *Spodoptera frugiperda* cells using a modified Bac-to-Bac system (Invitrogen). The MBPTrap column (GE Healthcare) was used to purify the recombinant protein according to the manufacturer's instruction. Ultracentrifuge and gel filtration were used to finally remove the aggregates and obtain the pure protein (Supplemental Experimental Procedures).

Supplemental Information

Supplemental Information includes four figures, Supplemental Results, and Supplemental Experimental Procedures and can be found with this article online at <http://dx.doi.org/10.1016/j.cub.2013.03.065>.

Acknowledgments

The authors thank Iain Patten, Joshua Alper, Hugo Bowne-Anderson, Fernando Carrillo Oesterreich, Mohammed Mahamdeh, and Elisabeth Knust for their comments on the manuscript; Wieland Huttner for the support on the work with electron microscopy; Martin Göpfert for *nompC* mutant strains; and Heike Petzold for the general lab organization. Special thanks to the protein expression facility, antibody facility, electron microscopy facility, and light microscopy facility at MPI-CBG for their technical support. We acknowledge our funding from the Max-Planck Society. X.L. was supported by a postdoctoral fellowship from the Alexander von Humboldt Foundation (2009–2011). R.G. was supported by the German Science Foundation under grant Vo899/6.

Received: November 8, 2012

Revised: February 22, 2013

Accepted: March 26, 2013

Published: April 11, 2013

References

1. Lumpkin, E.A., Marshall, K.L., and Nelson, A.M. (2010). The cell biology of touch. *J. Cell Biol.* 191, 237–248.
2. Chalfie, M. (2009). Neurosensory mechanotransduction. *Nat. Rev. Mol. Cell Biol.* 10, 44–52.
3. Gillespie, P.G., and Müller, U. (2009). Mechanotransduction by hair cells: models, molecules, and mechanisms. *Cell* 139, 33–44.
4. Gillespie, P.G., and Walker, R.G. (2001). Molecular basis of mechanosensory transduction. *Nature* 413, 194–202.
5. Corey, D.P., and Hudspeth, A.J. (1983). Kinetics of the receptor current in bullfrog saccular hair cells. *J. Neurosci.* 3, 962–976.
6. Albert, J.T., Nadrowski, B., and Göpfert, M.C. (2007). Mechanical signatures of transducer gating in the *Drosophila* ear. *Curr. Biol.* 17, 1000–1006.
7. Howard, J., and Hudspeth, A.J. (1988). Compliance of the hair bundle associated with gating of mechano-electrical transduction channels in the bullfrog's saccular hair cell. *Neuron* 1, 189–199.
8. Holton, T., and Hudspeth, A.J. (1986). The transduction channel of hair cells from the bull-frog characterized by noise analysis. *J. Physiol.* 375, 195–227.
9. Pickles, J.O., Comis, S.D., and Osborne, M.P. (1984). Cross-links between stereocilia in the guinea pig organ of Corti, and their possible relation to sensory transduction. *Hear. Res.* 15, 103–112.
10. Kazmierczak, P., Sakaguchi, H., Tokita, J., Wilson-Kubalek, E.M., Milligan, R.A., Müller, U., and Kachar, B. (2007). Cadherin 23 and protocadherin 15 interact to form tip-link filaments in sensory hair cells. *Nature* 449, 87–91.
11. Sotomayor, M., Corey, D.P., and Schulten, K. (2005). In search of the hair-cell gating spring elastic properties of ankyrin and cadherin repeats. *Structure* 13, 669–682.
12. Siemens, J., Lillo, C., Dumont, R.A., Reynolds, A., Williams, D.S., Gillespie, P.G., and Müller, U. (2004). Cadherin 23 is a component of the tip link in hair-cell stereocilia. *Nature* 428, 950–955.

13. Powers, R.J., Roy, S., Atilgan, E., Brownell, W.E., Sun, S.X., Gillespie, P.G., and Spector, A.A. (2012). Stereocilia membrane deformation: implications for the gating spring and mechanotransduction channel. *Biophys. J.* *102*, 201–210.
14. Kachar, B., Parakkal, M., Kurc, M., Zhao, Y., and Gillespie, P.G. (2000). High-resolution structure of hair-cell tip links. *Proc. Natl. Acad. Sci. USA* *97*, 13336–13341.
15. Pickles, J.O., Rouse, G.W., and von Perger, M. (1991). Morphological correlates of mechanotransduction in acousticolateral hair cells. *Scanning Microsc.* *5*, 1115–1124, discussion 1124–1118.
16. Cueva, J.G., Mulholland, A., and Goodman, M.B. (2007). Nanoscale organization of the MEC-4 DEG/ENAC sensory mechanotransduction channel in *Caenorhabditis elegans* touch receptor neurons. *J. Neurosci.* *27*, 14089–14098.
17. Keil, T.A. (1997). Functional morphology of insect mechanoreceptors. *Microsc. Res. Tech.* *39*, 506–531.
18. Thurm, U., Erler, G., Gödde, J., Kastrup, H., Keil, T., Völker, W., and Vohwinkel, B. (1983). Cilia specialized for Mechanoreception. *J. Submicrosc. Cytol.* *15*, 151–155.
19. Voelker, W. (1982). Lebendbeobachtungen an kutikulaeren Reizübertragungsstrukturen campaniformer Sensillen und Hochauflösungs-Elektronenmikroskopie der reizaufnehmenden Sinneszellregion. PhD thesis, Westfälische Wilhelms-Universität, Münster, Germany.
20. Yan, Z., Zhang, W., He, Y., Gorczyca, D., Xiang, Y., Cheng, L.E., Meltzer, S., Jan, L.Y., and Jan, Y.N. (2013). *Drosophila* NOMPC is a mechanotransduction channel subunit for gentle-touch sensation. *Nature* *493*, 221–225.
21. Walker, R.G., Willingham, A.T., and Zuker, C.S. (2000). A *Drosophila* mechanosensory transduction channel. *Science* *287*, 2229–2234.
22. Lehnert, B.P., Baker, A.E., Gaudry, Q., Chiang, A.S., and Wilson, R.I. (2013). Distinct roles of TRP channels in auditory transduction and amplification in *Drosophila*. *Neuron* *77*, 115–128.
23. Howard, J., and Bechstedt, S. (2004). Hypothesis: a helix of ankyrin repeats of the NOMPC-TRP ion channel is the gating spring of mechanoreceptors. *Curr. Biol.* *14*, R224–R226.
24. Lee, G., Abdi, K., Jiang, Y., Michaely, P., Bennett, V., and Marszalek, P.E. (2006). Nanospring behaviour of ankyrin repeats. *Nature* *440*, 246–249.
25. Effertz, T., Nadrowski, B., Piepenbrock, D., Albert, J.T., and Göpfert, M.C. (2012). Direct gating and mechanical integrity of *Drosophila* auditory transducers require TRPN1. *Nat. Neurosci.* *15*, 1198–1200.
26. Effertz, T., Wiek, R., and Göpfert, M.C. (2011). NompC TRP channel is essential for *Drosophila* sound receptor function. *Curr. Biol.* *21*, 592–597.
27. Göpfert, M.C., Albert, J.T., Nadrowski, B., and Kamikouchi, A. (2006). Specification of auditory sensitivity by *Drosophila* TRP channels. *Nat. Neurosci.* *9*, 999–1000.
28. Cheng, L.E., Song, W., Looger, L.L., Jan, L.Y., and Jan, Y.N. (2010). The role of the TRP channel NompC in *Drosophila* larval and adult locomotion. *Neuron* *67*, 373–380.
29. Li, J., Mahajan, A., and Tsai, M.D. (2006). Ankyrin repeat: a unique motif mediating protein-protein interactions. *Biochemistry* *45*, 15168–15178.
30. Liang, X., Madrid, J., Saleh, H.S., and Howard, J. (2011). NOMPC, a member of the TRP channel family, localizes to the tubular body and distal cilium of *Drosophila* campaniform and chordotonal receptor cells. *Cytoskeleton (Hoboken)* *68*, 1–7.
31. Spinola, S.M., and Chapman, K.M. (1975). Proprioceptive indentation of the campaniform sensilla of cockroach legs. *J. Comp. Physiol. A Neuroethol. Sens. Neural Behav. Physiol.* *96*, 257–272.
32. Michaely, P., Tomchick, D.R., Machius, M., and Anderson, R.G. (2002). Crystal structure of a 12 ANK repeat stack from human ankyrinR. *EMBO J.* *21*, 6387–6396.
33. Lee, J., Moon, S., Cha, Y., and Chung, Y.D. (2010). *Drosophila* TRPN(=NOMPC) channel localizes to the distal end of mechanosensory cilia. *PLoS ONE* *5*, e11012.
34. Chen, Z., and Rand, R.P. (1997). The influence of cholesterol on phospholipid membrane curvature and bending elasticity. *Biophys. J.* *73*, 267–276.
35. Leikin, S., Kozlov, M.M., Fuller, N.L., and Rand, R.P. (1996). Measured effects of diacylglycerol on structural and elastic properties of phospholipid membranes. *Biophys. J.* *71*, 2623–2632.
36. Howard, J. (2001). *Mechanics of Motor Proteins and the Cytoskeleton* (Sunderland, MA, USA: Sinauer Associates).
37. Venken, K.J., Carlson, J.W., Schulze, K.L., Pan, H., He, Y., Spokony, R., Wan, K.H., Koriabine, M., de Jong, P.J., White, K.P., et al. (2009). Versatile P[acman] BAC libraries for transgenesis studies in *Drosophila melanogaster*. *Nat. Methods* *6*, 431–434.
38. McLachlan, A.D., and Karn, J. (1983). Periodic features in the amino acid sequence of nematode myosin rod. *J. Mol. Biol.* *164*, 605–626.